Highly anisotropic surface resonance states in a kagome semimetal

$Ni_3In_2Se_2$

K. Y. Zhai[1], X. Du[1], C. Chen[3,4,5], W. J. Shi[6,7], W. X. Zhao[1], Y. D. Li[1], Z. K. Liu[3,4], Y. Y. Lv[2*], Y. L. Chen[1,3,4,8*], L. X. Yang[1,9*]

[1]*State Key Laboratory of Low Dimensional Quantum Physics, Department of Physics, Tsinghua University, Beijing 100084, China.*

[2]*National Laboratory of Solid State Microstructures, Department of Materials Science and Engineering, Nanjing University, Nanjing, China.*

[3]*School of Physical Science and Technology, ShanghaiTech University and CAS-Shanghai Science Research Center, Shanghai 201210, China.*

[4]*ShanghaiTech Laboratory for Topological Physics, Shanghai 200031, China.*

[5]*Advanced Light Source, Lawrence Berkeley National Laboratory, Berkeley, California 94720, USA*

[6]*Center for Transformative Science, ShanghaiTech University, Shanghai, 201210, China*

[7]*Shanghai High Repetition Rate XFEL and Extreme Light Facility (SHINE), ShanghaiTech University, Shanghai, 201210, China*

[8]*Department of Physics, Clarendon Laboratory, University of Oxford, Parks Road, Oxford OX1 3PU, UK.*

[9]*Frontier Science Center for Quantum Information, Beijing 100084, China.*

[‡]*Email address: LXY: lxyang@tsinghua.edu.cn, YLC: yulin.chen@physics.ox.ac.uk, YYLv: lvyangws0801@nju.edu.cn*

Shandite kagome materials have attracted great research attention due to their intriguing properties, such as magnetic Weyl semimetal phase, endless nodal lines, and pressure-induced superconductivity. In this work, by combining angle-resolved photoemission spectroscopy and *ab initio* calculation, we systematically investigate the electronic band structure of the shandite kagome compound $Ni_3In_2Se_2$. The measured band structure is in good agreement with ab-initio calculation with spin-orbital coupling effect. The experimental spectra are predominantly characterized by surface resonance states exhibiting highly anisotropic band dispersions near the Fermi level. These features dominate the electronic states near E_F, which are likely associated with the anisotropic transport properties observed in $Ni_3In_2Se_2$. Notably, the large spin-orbit coupling in this material leads to the formation of a massive Dirac-like band dispersion in the surface resonance states, contrasting with the gapless Dirac dispersion found in the surface states of its sister compound $Ni_3In_2S_2$. Our experiments will help understand the influence of spin-orbit coupling effect on both the surface and bulk electronic states of shandite compounds. Furthermore, it establishes a foundation for exploring the potential applications of surface resonance states in surface science.

I. INTRODUCTION

The geometric structure of a crystal lattice plays a pivotal role in the electronic properties of quantum materials. A prominent example is the kagome lattice, a two-dimensional (2D) network of corner-sharing triangles, which hosts a variety of characteristic electronic features such as flat bands, van Hove singularities, and Dirac fermions [1-19]. The interplay between lattice geometry, magnetism, topology, and electronic structure gives rise to rich intriguing properties of kagome materials, such as the magnetic frustrated quantum spin liquid [20-22], fractional quantum Hall state [23-26], quantum anomalous Hall effect [27-29], novel topological quantum phases [1-7,30], and many-body emergent properties [31-40].

Among many kagome materials, shandite kagome compounds attracted particular interests due to their rich tunability and rare synergy of magnetism, topology, and correlation. For instance, ferromagnetic Weyl semimetal $Co_3Sn_2S_2$ exhibits giant anomalous Hall effect [41-44]; $Pd_3Pb_2Se_2$ becomes superconducting under pressure [40]; Recently, endless Dirac nodal lines have been predicted in shandites $Ni_3In_2S_2$ and $Ni_3In_2Se_2$ with record-high carrier mobility among kagome materials [45,46]. The electronic structure of the former has been investigated by angle-resolved photoemission spectroscopy (ARPES) to confirm the existence of Dirac nodal lines [45], while the electronic structure of $Ni_3In_2Se_2$ with stronger spin-orbit coupling (SOC) remains to be experimentally investigated.

Here, we systematically study the electronic structure of the shandite kagome compound $Ni_3In_2Se_2$ using high-resolution ARPES and ab-initio calculations. Contrary to expectations for kagome lattice, we do not observe kagome-related electronic structure, similar to other shandite compounds in previous studies [41-46]. The experimental spectra, in agreement with

the ab-initio calculation, are predominantly influenced by the surface resonance states (SRSs). These SRSs are well reproduced by the calculated bulk band structure except that they exhibit weak k_z dispersion. Notably, the SRSs form highly anisotropic massive Dirac-like band dispersions, which may be pivotal to the in-plane transport behaviors and linked to the anisotropic transport properties observed in the system. Our findings establish shandite compound $Ni_3In_2Se_2$ as a promising platform for exploring the application of SRSs in kagome materials with large SOC effect, particularly in surface chemistry and surface catalysis.

II. METHODS

Crystal Growth: Single crystals of $Ni_3In_2Se_2$ were grown by using a melt solidification method. The high-purity reagents Ni (Aladdin, 99.9%), In (Aladdin, 99.99%), and Se (Alfa Aesar, 99.999%) powders were mixed with a molar ratio of Ni:In:Se = 3:2:2. The mixture was sealed into an evacuated (10^{-4} Pa) quartz tube and heated in a box furnace to 850 °C in 10 h. It is then held at this temperature for 24 h, and subsequently cooled down to 750 °C at a rate of 1°C/h. Excessive flux on the crystal surface was removed by centrifuging at this temperature. Plate-like $Ni_3In_2Se_2$ single crystals with metallic luster can be obtained.

ARPES: ARPES measurements were performed at the beamline 5-2 of the Stanford Synchrotron Radiation Lightsource (SSRL) and beamline 10.0.1 of the Advanced Light Source (ALS) with Scienta DA30 and R4000 analyzers, respectively. The total energy and angular resolutions were set to 10 meV and 0.2°, respectively. Laser-based ARPES experiments were performed at Tsinghua University using a 7 eV laser and Scienta DA 30 analyser. The total energy and angular resolutions were about 4 meV and 0.2°, respectively. The samples were cleaved *in situ* and measured in ultrahigh vacuum below 5×10^{-11} Torr.

Theoretical Calculation: We performed the first-principles calculations using the Vienna ab initio Simulation Package (VASP) [47]. The interactions between the valence electrons and ion cores were described by the projector augmented wave method [48,49], and exchange-correlation potential is formulated by the generalized gradient approximation with the Perdew-Burke-Ernzerhof (PBE) scheme [47]. The kinetic energy cutoff for the plane-wave basis was set to 366 eV. The Γ-centered 10×10×10 k points were used for the first Brillouin-zone sampling. The spin-orbit coupling (SOC) was included in all the calculations. The lattice was fully relaxed until the force is less than 0.01 eV/A. The lattice constants after relaxation are a = 5.416 Å and c = 14.206 Å (conventional unit cell), which are close to the experimental values [50]. The tight-binding Hamiltonian was constructed using the maximally localized Wannier functions with Se *p*, Ni *d*, and In *s* and *p* orbitals which were provided by Wannier90 package [51]. The surface states were calculated by the surface Green's function method [52] based the tight-binding Hamiltonian.

III. RESULTS AND DISCUSSION

The shandite semimetal $Ni_3In_2Se_2$ crystallizes into a rhombohedral structure with space group No.166 ($R\bar{3}m$). In the conventional cell of $Ni_3In_2Se_2$ [Fig. 1(a)], the Ni atoms in the Ni_3-In layer form a 2D kagome lattice [Fig. 1(b)], which stacks in ABC sequence along the c direction. The adjacent kagome layers are separated by an In-Se layer. Figures 1(c) and 1(d) show the primitive unit cell and corresponding 3D Brillouin zone (BZ), respectively. The 2D projection of the BZ on the (001) surface is also shown in Fig. 1(d). Figures 1(e) and 1(f) compare the ab-initio calculations of the band structure of $Ni_3In_2Se_2$ along high symmetry

directions with and without spin-orbit coupling (SOC). Without SOC, there are two band crossings along the *TH* and Γ*S* directions, which locate above and below E_F, respectively. According to the symmetry analysis, the band crossings extend along the (111) direction, forming endless Dirac nodal lines [46,53]. The Dirac nodal lines survive the weak SOC effect in $Ni_3In_2S_2$, which is believed to be crucial for its giant magnetoresistance [45]. In $Ni_3In_2Se_2$, the large SOC effect lifts the degeneracy of the band crossings and eliminates the Dirac nodal lines, as indicated by the red circles in Fig. 1(f). Nevertheless, previous theoretical studies suggest that $Ni_3In_2Se_2$ may still exhibit nontrivial topological characteristics even with SOC included [46].

Using high-resolution ARPES, we acquire high-quality data of the electronic structure of $Ni_3In_2Se_2$ in Fig. 2. The experimental electronic structure measured with 106 eV photons strongly depends on the photon polarization. The linear-horizontally (LH) and linear-vertically (LV) polarized photons highlight different features in the experimental Fermi surface (FS), since the electronic states near the Fermi level (E_F) are dominated by Ni 3*d* electrons. Notably, a small triangular electron pocket near the $\overline{K}$ point is resolved under LH polarization, while a line-like feature emerges around the $\overline{M}$ point under LV polarization. Figures 2(b) and 2(c) show the experimental band dispersions along high-symmetry directions. We observe a shallow and tiny electron band (α) at the $\overline{K}$ point and a nearly dispersionless band (β) along the $\overline{\Gamma}\,\overline{M}$ direction. Besides, there exists blurred spectral weight near E_F along the $\overline{\Gamma}\,\overline{K}$ direction, contributing to the broad features between the $\overline{\Gamma}$ and $\overline{K}$ points on the FS [Fig. 2(a)].

To better compare the experimental electronic structure with the calculated results, we sum the data collected using LH- and LV-polarized photons at 53 eV. The FS in Fig. 2(d) exhibits hexagonal symmetry with main features consistent with those in Fig. 2(a). The experimental band dispersions along $\overline{\Gamma}\,\overline{K}\,\overline{M}$ are in good consistence with the surface-projected calculation, as compared in Figs. 2(e) and 2(f). It is noteworthy that, despite the kagome lattice formed by Ni atoms, our ARPES data show no signatures of the characteristic kagome-derived electronic features (e.g., flat bands or Dirac cones originating purely from the kagome network), similar to other shandite kagome materials [41,45].

In Fig. 2 (e), there are three bands (α, β, and γ) show prominent intensity compared to other broad and weak spectral features. By comparing with the calculation in Fig. 2(f), it turns out that they reflect the upper envelops of the surface-projected bulk band dispersions with substantial k_z dispersion.

However, these prominent experimental features show minor change at different photon energies, contrasting to the behavior of bulk electronic states [Figs. 2(b), 2(c), and 2(e)]. To further verify their origin, we conducted detailed photon-energy dependent measurements as shown in Fig. 3. Despite the clear k_z dispersion in the calculation [Fig. 2(f)], ~~our measurement of the FS in the k_y-k_z plane reveals k_z variation only around the $\overline{\Gamma}$ point as depicted in Fig. 3(a), while the spectra near k_y = 1.16 Å^{-1} (the $\overline{M}$ point) exhibits line-like features in a large rang of k_z [Fig. 3(a)].~~ the electronic states near $\overline{M}$ and $\overline{K}$ show weak k_z variation [Fig. 3(a)]. The bottom of the β band and the top of the γ band remain nearly unchanged with k_z, as indicated by the black arrows in Fig. 3(b). Figures 3(c-g) display the band dispersions along the $\overline{\Gamma}\,\overline{K}\,\overline{M}$ direction measured at different photon energies. The α, β, and γ bands consistently

show strong intensity and negligible dispersion with photon energy, which contrasts with the strong k_z dependence predicted in the calculations in Fig. 2(f). Taken together, these experimental observations and theoretical comparisons strongly indicate that the α, β, and γ bands originate from SRSs.

Except for the α, β, and γ bands, there also exist broad and weak electronic states near $\overline{\Gamma}$ and $\overline{M}$, showing pronounced photon-energy dependence, which are attributed to the bulk states. The bulk electronic states form an electron band near $\overline{M}$, with band bottom at about -500 meV (-125 meV) measured at 103 eV (125 eV). The electronic states near $\overline{\Gamma}$, however, is strongly suppressed due to the matrix element effect. ~~In contrast, a broad electron-like band appears near $\overline{M}$, showing pronounced photon-energy dependence (marked by red arrows in Fig. 3(c-g), which we attribute to a bulk electronic state.~~ To further probe the bulk bands near $\overline{\Gamma}$, we present laser-ARPES data measured using a 7 eV laser in Fig. 3(h), which probes deeper in the sample bulk. In contrast to the electron-like band dispersion near $\overline{\Gamma}$ measured using synchrotron-based ARPES, here we observe a weakly dispersive hole-like band around $\overline{\Gamma}$, together with a dispersive hole-like band with band top around 75 meV. This result is in agreement with the calculated band structure near the *T* point [Fig. 1(f)], suggesting that the 7 eV laser probes the k_z position near the *T* point. Moreover, the two bands are degenerate at the *T* point in the calculation without SOC in Fig 1(e). The observed band splitting in the laser-ARPES data thus confirms the large SOC effect in $Ni_3In_2Se_2$. ~~Given the larger probing depth of laser-ARPES, it is reasonable to attribute these features to bulk electronic states.~~ Similar band dispersions are also visible in the 119 eV data [Fig. 3(f)], though with significantly weaker intensity compared to the dominant SRSs.

The β and γ bands form a massive Dirac-like dispersion along $\overline{K}\,\overline{M}\,\overline{K}$ with a gap of about 180 meV. Along $\overline{\Gamma}\,\overline{M}$, the β band contributes the line-like FS [Figs. 2(a) and 2(d)], suggesting highly anisotropic dispersions of the SRSs. Figure 4(a) shows the band structure along $\overline{K}\,\overline{M}\,\overline{K}$ at different k_x positions, which remains a massive Dirac-like dispersion. Therefore, the SRSs form quasi-1D dispersions with nearly flat band top (bottom) along $\overline{\Gamma}\,\overline{M}$, as shown in Fig. 4(b). We estimate the effective masses of the upper and lower branches of the massive Dirac-like band along different directions, which results in $m_e^{\prime}=26.7\,m_e\,(m_h^{\prime}=-6.6\,m_e)$ along $\overline{\Gamma}\,\overline{M}$, and $m_e^{\prime}=0.23\,m_e\,(m_h^{\prime}=-0.2\,m_e)$ along $\overline{K}\,\overline{M}\,\overline{K}$. To our best knowledge, such a large anisotropy of the carrier effective mass is uncommon in 3D compounds. It is noteworthy that the SRSs reflect the bulk states, and the bulk bands exhibit similar anisotropy in the effective mass, as demonstrated by the calculation in Figs. 1(f) and 2(f). ~~This anisotropy may be linked to the anisotropic transport properties of $Ni_3In_2Se_2$ [54].~~

Finally, it is informative to compare the band structure of $Ni_3In_2Se_2$ and $Ni_3In_2S_2$. The previous ARPES investigation of $Ni_3In_2S_2$ has revealed a gapless Dirac band near $\overline{M}$ ~~that is relevant to the high mobility and large magnetoresistance of $Ni_3In_2S_2$~~ [55]. In drastic contrast, $Ni_3In_2Se_2$ exhibits a substantial energy gap of ~180 meV, as evidenced by the band dispersions along the $\overline{K}\,\overline{M}\,\overline{K}$ direction in Fig. 4(c). This discrepancy arises from the different bulk band gap near $\overline{M}$, possibly due to the different lattice parameters and SOC effects in the two compounds.

In conclusion, we have systematically investigated the electronic structure of $Ni_3In_2Se_2$ with a

kagome lattice. We observe prominent SRSs forming a highly anisotropic massive Dirac-like band dispersion around the $\overline{M}$ point. The SRSs in a kagome material with large SOC effect may be promising for the application in surface chemistry and catalysis.

ACKNOWLEDGMENT

We thank D. H. Lu, M. Hashimoto and S.-K. Mo for their beamline assistance at SSRL and ALS. This work is funded by the National Natural Science Foundation of China (Grants No. No. 12275148 and No. 92365204) and the National Key R&D Program of China (Grants No. 2022YFA1403100 and No. 2022YFA1403200). The experiments at SSRL and ALS are supported by the US Department of Energy (DoE) Office of Basic Energy Science under contract no. DE-AC02-76SF00515 and no. DE-AC02-05CH11231.

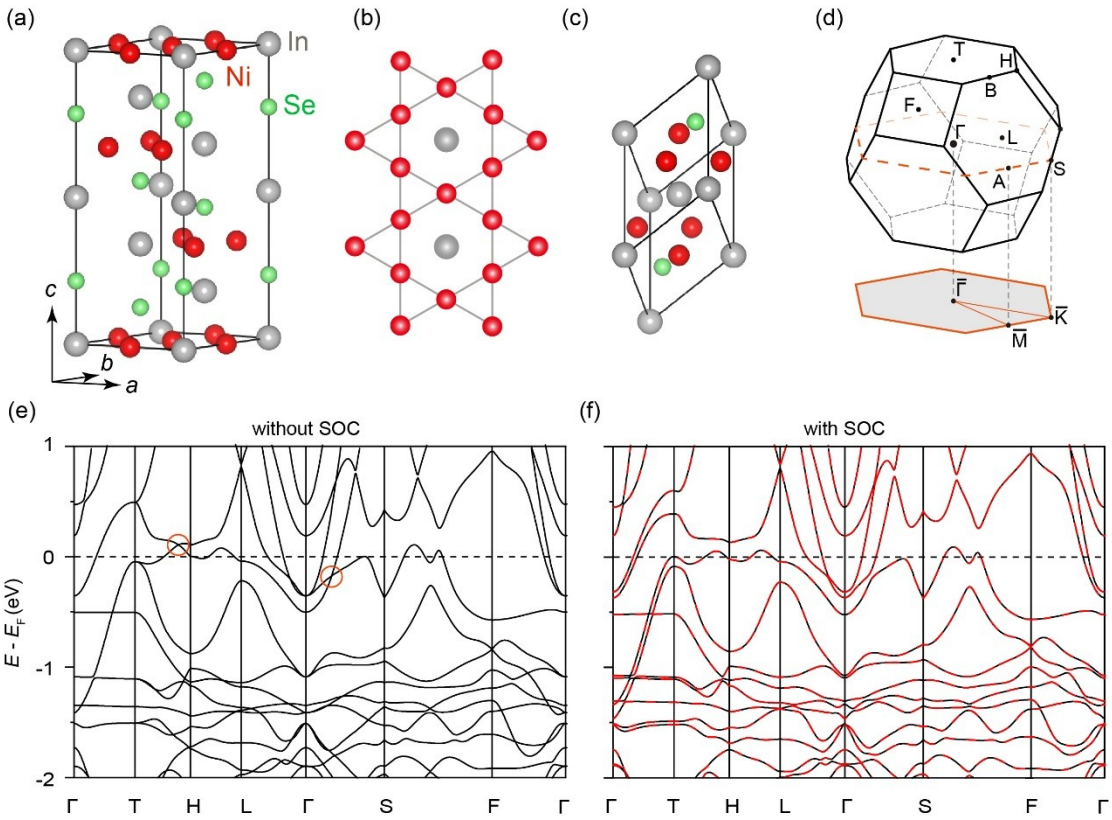

FIG. 1. Crystal structure and calculated band structure of $Ni_3In_2Se_2$. (a)-(c) Schematic illustration of (a) the conventional unit cell, (b) the kagome layer formed by Ni atoms, and (c) the primitive unit cell. (d) 3D Brillouin zone corresponding to the primitive cell together with its surface projection. (e), (f) Calculated band structure without (e) and with (f) spin-orbit coupling (SOC). The red dashed curves are the Wannier fitting of the energy bands.

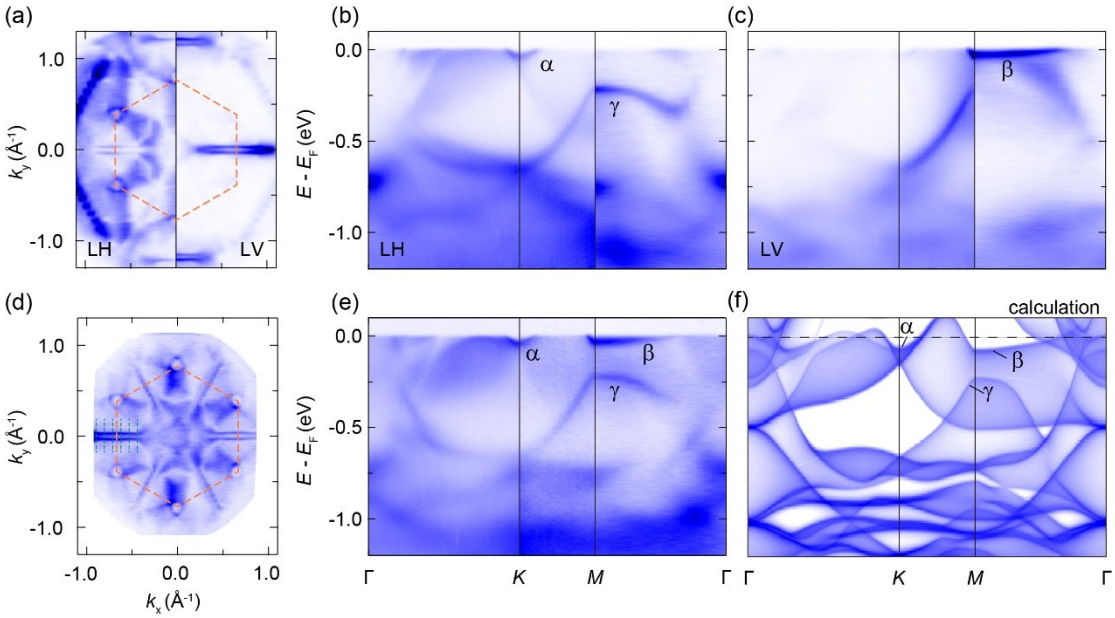

FIG. 2. The basic band structure of $Ni_3In_2Se_2$ measured with synchrotron-based ARPES. (a) Fermi surface (FS) measured with linear-horizontally (LH, left) and linear-vertically (LV, right) polarized photons at 106 eV. The orange dashed hexagon is the first surface BZ. (b), (c) Band structure along high-symmetry directions measured with LH- and LV-polarized photons at 106 eV, respectively. (d), (e) FS and band dispersions obtained by summing up the data collected using LH- and LV-polarized photons at 54 eV. (f) Calculated bulk band structure projected on the (001) surface.

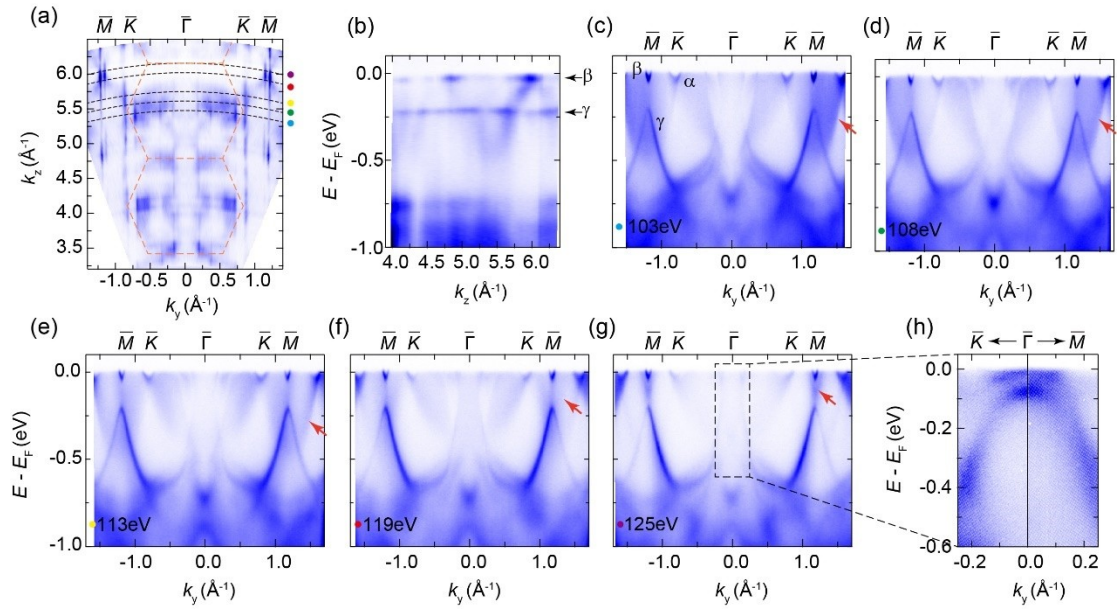

FIG. 3. Band structure measured at different photon energies. (a) FS map in the k_y-k_z plane. (b) Band dispersion along k_z at k_y = 1.16 Å^{-1}. (c-g) Band dispersions along the $\bar{\Gamma}\bar{K}\bar{M}$ direction measured at different photon energies. (h) Laser-ARPES spectra near the $\bar{\Gamma}$ point.

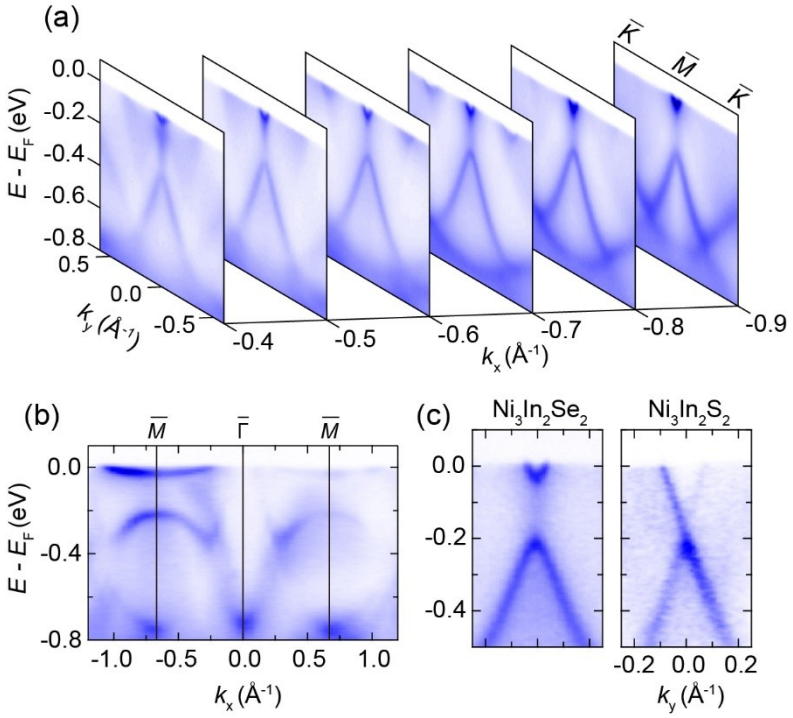

FIG. 4. Anisotropic massive Dirac band. (a), (b) Dispersion of the β and γ bands along (a) $\overline{K}\,\overline{M}\,\overline{K}$ at different k_x positions and (b) $\overline{M}\,\overline{\Gamma}\,\overline{M}$. (c) Comparison between the massive SRS and massless surface states in $Ni_3In_2Se_2$ and $Ni_3In_2S_2$.

Reference

[1] J.-X. Yin, B. Lian, and M. Z. Hasan, *Topological kagome magnets and superconductors*, Nature **612**, 647 (2022).

[2] Y. Wang, H. Wu, G. T. McCandless, J. Y. Chan, and M. N. Ali, *Quantum states and intertwining phases in kagome materials*, Nat. Rev. Phys. **5**, 635 (2023).

[3] S. D. Wilson and B. R. Ortiz, *AV3Sb5 kagome superconductors*, Nat. Rev. Mater. **9**, 420 (2024).

[4] K. Jiang, T. Wu, J.-X. Yin, Z. Wang, M. Z. Hasan, S. D. Wilson, X. Chen, and J. Hu, *Kagome superconductors AV_3Sb_5 (A = K, Rb, Cs)*, Nat. Sci. Rev. **10**, nwac199 (2022).

[5] M. Li, H. Ma, R. Lou, and S. Wang, *Electronic band structures of topological kagome materials*, Chin. Phys. B **34**, 017101 (2025).

[6] Y. Hu, X. Wu, A. P. Schnyder, and M. Shi, *Electronic landscape of kagome superconductors AV3Sb5 (A = K, Rb, Cs) from angle-resolved photoemission spectroscopy*, npj Quantum Materials **8**, 67 (2023).

[7] X. Gu, C. Chen, W. S. Wei, L. L. Gao, J. Y. Liu, X. Du, D. Pei, J. S. Zhou, R. Z. Xu, Z. X. Yin *et al.*, *Robust kagome electronic structure in the topological quantum magnets XMn_6Sn_6 (X=Dy,Tb,Gd,Y)*, Phys. Rev. B **105**, 155108 (2022).

[8] L. Ye, M. Kang, J. Liu, F. von Cube, C. R. Wicker, T. Suzuki, C. Jozwiak, A. Bostwick, E. Rotenberg, D. C. Bell *et al.*, *Massive Dirac fermions in a ferromagnetic kagome metal*, Nature **555**, 638 (2018).

[9] M. Li, Q. Wang, G. Wang, Z. Yuan, W. Song, R. Lou, Z. Liu, Y. Huang, Z. Liu, H. Lei *et al.*, *Dirac cone, flat band and saddle point in kagome magnet YMn_6Sn_6*, Nat. Commun. **12**, 3129 (2021).

[10] X. Teng, J. S. Oh, H. Tan, L. Chen, J. Huang, B. Gao, J.-X. Yin, J.-H. Chu, M. Hashimoto, D. Lu *et al.*, *Magnetism and charge density wave order in kagome FeGe*, Nat. Phys. **19**, 814 (2023).

[11] Z. Jiang, Z. Liu, H. Ma, W. Xia, Z. Liu, J. Liu, S. Cho, Y. Yang, J. Ding, J. Liu *et al.*, *Flat bands, non-trivial band topology and rotation symmetry breaking in layered kagome-lattice* $RbTi_3Bi_5$, Nat. Commun. **14**, 4892 (2023).

[12] K. Kuroda, T. Tomita, M. T. Suzuki, C. Bareille, A. A. Nugroho, P. Goswami, M. Ochi, M. Ikhlas, M. Nakayama, S. Akebi *et al.*, *Evidence for magnetic Weyl fermions in a correlated metal*, Nat. Mater. **16**, 1090 (2017).

[13] Z. Sun, H. Zhou, C. Wang, S. Kumar, D. Geng, S. Yue, X. Han, Y. Haraguchi, K. Shimada, P. Cheng *et al.*, *Observation of Topological Flat Bands in the Kagome Semiconductor* Nb_3Cl_8, Nano Letters **22**, 4596 (2022).

[14] D. Di Sante, C. Bigi, P. Eck, S. Enzner, A. Consiglio, G. Pokharel, P. Carrara, P. Orgiani, V. Polewczyk, J. Fujii *et al.*, *Flat band separation and robust spin Berry curvature in bilayer kagome metals*, Nat. Phys. **19**, 1135 (2023).

[15] Z. Lin, J.-H. Choi, Q. Zhang, W. Qin, S. Yi, P. Wang, L. Li, Y. Wang, H. Zhang, Z. Sun *et al.*, *Flatbands and Emergent Ferromagnetic Ordering in* Fe_3Sn_2 *Kagome Lattices*, Phys. Rev. Lett. **121**, 096401 (2018).

[16] M. Kang, L. Ye, S. Fang, J.-S. You, A. Levitan, M. Han, J. I. Facio, C. Jozwiak, A. Bostwick, E. Rotenberg *et al.*, *Dirac fermions and flat bands in the ideal kagome metal FeSn*, Nat. Mater. **19**, 163 (2020).

[17] M. Kang, S. Fang, L. Ye, H. C. Po, J. Denlinger, C. Jozwiak, A. Bostwick, E. Rotenberg, E. Kaxiras, J. G. Checkelsky *et al.*, *Topological flat bands in frustrated kagome lattice CoSn*,

Nat. Commun. **11**, 4004 (2020).

[18] Z. Liu, M. Li, Q. Wang, G. Wang, C. Wen, K. Jiang, X. Lu, S. Yan, Y. Huang, D. Shen *et al.*, *Orbital-selective Dirac fermions and extremely flat bands in frustrated kagome-lattice metal CoSn*, Nat. Commun. **11**, 4002 (2020).

[19] S. Peng, Y. Han, G. Pokharel, J. Shen, Z. Li, M. Hashimoto, D. Lu, B. R. Ortiz, Y. Luo, H. Li *et al.*, *Realizing Kagome Band Structure in Two-Dimensional Kagome Surface States of* RV_6Sn_6 *(R = Gd, Ho)*, Phys. Rev. Lett. **127**, 266401 (2021).

[20] L. Balents, *Spin liquids in frustrated magnets*, Nature **464**, 199 (2010).

[21] T. H. Han, J. S. Helton, S. Chu, D. G. Nocera, J. A. Rodriguez-Rivera, C. Broholm, and Y. S. Lee, *Fractionalized excitations in the spin-liquid state of a kagome-lattice antiferromagnet*, Nature **492**, 406 (2012).

[22] M. Fu, T. Imai, T. H. Han, and Y. S. Lee, *Evidence for a gapped spin-liquid ground state in a kagome Heisenberg antiferromagnet*, Science **350**, 655 (2015).

[23] Z. Liu, F. Liu, and Y.-S. Wu, *Exotic electronic states in the world of flat bands: From theory to material*, Chinese Physics B **23** (2014).

[24] D. N. Sheng, Z. C. Gu, K. Sun, and L. Sheng, *Fractional quantum Hall effect in the absence of Landau levels*, Nat. Commun. **2**, 389 (2011).

[25] T. Neupert, L. Santos, C. Chamon, and C. Mudry, *Fractional Quantum Hall States at Zero Magnetic Field*, Phys. Rev. Lett. **106**, 236804 (2011).

[26] E. Tang, J. W. Mei, and X. G. Wen, *High-temperature fractional quantum Hall states*, Phys. Rev. Lett. **106**, 236802 (2011).

[27] G. Xu, B. Lian, and S. C. Zhang, *Intrinsic Quantum Anomalous Hall Effect in the Kagome Lattice Cs2LiMn3F12*, Phys. Rev. Lett. **115**, 186802 (2015).

[28] K. Ohgushi, S. Murakami, and N. Nagaosa, *Spin anisotropy and quantum Hall effect in thekagomélattice: Chiral spin state based on a ferromagnet*, Phys. Rev. B **62**, R6065 (2000).

[29] W. Zhu, S. S. Gong, T. S. Zeng, L. Fu, and D. N. Sheng, *Interaction-Driven Spontaneous Quantum Hall Effect on a Kagome Lattice*, Phys. Rev. Lett. **117**, 096402 (2016).

[30] X. Zhang, L. Jin, X. Dai, and G. Liu, *Topological Type-II Nodal Line Semimetal and Dirac Semimetal State in Stable Kagome Compound Mg_3Bi_2*, J. Phys. Chem. Lett. **8**, 4814 (2017).

[31] M. L. Kiesel, C. Platt, and R. Thomale, *Unconventional Fermi Surface Instabilities in the Kagome Hubbard Model*, Phys. Rev. Lett. **110**, 126405 (2013).

[32] Y.-P. Lin and R. M. Nandkishore, *Complex charge density waves at Van Hove singularity on hexagonal lattices: Haldane-model phase diagram and potential realization in the kagome metals AV_3Sb_5 (A = K, Rb, Cs)*, Phys. Rev. B **104**, 045122 (2021).

[33] T. Park, M. Ye, and L. Balents, *Electronic instabilities of kagome metals: Saddle points and Landau theory*, Phys. Rev. B **104**, 035142 (2021).

[34] M. L. Kiesel and R. Thomale, *Sublattice interference in the kagome Hubbard model*, Phys. Rev. B **86**, 121105(R) (2012).

[35] X. Wu, T. Schwemmer, T. Muller, A. Consiglio, G. Sangiovanni, D. Di Sante, Y. Iqbal, W. Hanke, A. P. Schnyder, M. M. Denner *et al.*, *Nature of Unconventional Pairing in the Kagome Superconductors AV_3Sb_5 (A=K,Rb,Cs)*, Phys. Rev. Lett. **127**, 177001 (2021).

[36] X. Feng, K. Jiang, Z. Wang, and J. Hu, *Chiral flux phase in the Kagome superconductor AV_3Sb_5*, Sci. Bull. **66**, 1384 (2021).

[37] H. Tan, Y. Liu, Z. Wang, and B. Yan, *Charge Density Waves and Electronic Properties of Superconducting Kagome Metals*, Phys. Rev. Lett. **127**, 046401 (2021).

[38] Y. Li, Y. Liu, X. Du, S. Wu, W. Zhao, K. Zhai, Y. Hu, S. Zhang, H. Chen, J. Liu *et al.*, *Electron correlation and incipient flat bands in the Kagome superconductor* $CsCr_3Sb_5$, Nat. Commun. **16**, 3229 (2025).

[39] Y. Liu, Z.-Y. Liu, J.-K. Bao, P.-T. Yang, L.-W. Ji, S.-Q. Wu, Q.-X. Shen, J. Luo, J. Yang, J.-Y. Liu *et al.*, *Superconductivity under pressure in a chromium-based kagome metal*, Nature **632**, 1032 (2024).

[40] F. H. Yu, X. Y. Hua, T. Chen, J. Sun, M. Z. Shi, W. Z. Zhuo, D. H. Ma, H. H. Wang, J. J. Ying, and X. H. Chen, *Pressure-induced superconductivity in a shandite compound* $Pd_3Pb_2Se_2$ *with the Kagome lattice*, New J. Phys. **22**, 123013 (2020).

[41] D. F. Liu, A. J. Liang, E. K. Liu, Q. N. Xu, Y. W. Li, C. Chen, D. Pei, W. J. Shi, S. K. Mo, P. Dudin *et al.*, *Magnetic Weyl semimetal phase in a Kagomé crystal*, Science **365**, 1282 (2019).

[42] Q. Wang, Y. Xu, R. Lou, Z. Liu, M. Li, Y. Huang, D. Shen, H. Weng, S. Wang, and H. Lei, *Large intrinsic anomalous Hall effect in half-metallic ferromagnet* $Co_3Sn_2S_2$ *with magnetic Weyl fermions*, Nat. Commun. **9**, 3681 (2018).

[43] E. Liu, Y. Sun, N. Kumar, L. Muchler, A. Sun, L. Jiao, S. Y. Yang, D. Liu, A. Liang, Q. Xu *et al.*, *Giant anomalous Hall effect in a ferromagnetic Kagome-lattice semimetal*, Nat. Phys. **14**, 1125 (2018).

[44] Q. Xu, E. Liu, W. Shi, L. Muechler, J. Gayles, C. Felser, and Y. Sun, *Topological surface Fermi arcs in the magnetic Weyl semimetal* $Co_3Sn_2S_2$, Phys. Rev. B **97**, 235416 (2018).

[45] T. Zhang, T. Yilmaz, E. Vescovo, H. X. Li, R. G. Moore, H. N. Lee, H. Miao, S. Murakami, and M. A. McGuire, *Endless Dirac nodal lines in kagome-metal* $Ni_3In_2S_2$, npj Computational Materials **8**, 155 (2022).

[46] S. Kumar Pradhan, S. Pradhan, P. Mal, P. Rambabu, A. Lakhani, B. Das, B. Lingam Chittari, G. R. Turpu, and P. Das, *Endless Dirac nodal lines and high mobility in kagome semimetal $Ni_3In_2Se_2$: a theoretical and experimental study*, J. Phys.: Condens. Matter **36**, 445601 (2024).

[47] J. P, Perdew, K. Burke, and M. Ernzerhof, *Generalized Gradient Approximation Made Simple*, Phys. Rev. Lett. **77**, 3865 (1996).

[48] P. E. Blochl, *Projector augmented-wave method*, Phys. Rev. B **50**, 17953 (1994).

[49] G. Kresse and D. Joubert, *From ultrasoft pseudopotentials to the projector augmented-wave method*, Phys. Rev. B **59**, 1758 (1999).

[50] M. Zabel, S. Wandinger, and K.-J. Range, *Ternäre Chalkogenide $M_3M_2'X_2$ mit Shandit-Struktur / Ternary Chalcogenides $M_3M_2'X_2$ with Shandite-Type Structure*, Zeitschrift für Naturforschung B **34**, 238 (1979).

[51] I. Souza, N. Marzari, and D. Vanderbilt, *Maximally localized Wannier functions for entangled energy bands*, Phys. Rev. B **65**, 035109 (2001).

[52] M. P. L. Sancho, J. M. L. Sancho, and J. Rubio, *Highly convergent schemes for the calculation of bulk and surface Green functions*, J. Phys. F: Met. Phys **15**, 851 (1985).

[53] T. Zhang, T. Yilmaz, E. Vescovo, H. X. Li, R. G. Moore, H. N. Lee, H. Miao, S. Murakami, and M. A. McGuire, *Endless Dirac nodal lines in kagome-metal Ni3In2S2*, npj Computational Materials **8** (2022).

[54] L. Cao, G. Liu, Y. Zhang, Z. Yu, Y.-Y. Lv, S.-H. Yao, J. Zhou, Y. B. Chen, and Y.-F. Chen, *Crystal growth, transport, and magnetic properties of antiferromagnetic semimetal $Ni_3In_2Se_2$ crystals*, Phys. Rev. Mater. **7**, 084203 (2023).

[55] H. Fang, M. Lyu, H. Su, J. Yuan, Y. Li, L. Xu, S. Liu, L. Wei, X. Liu, H. Yang *et al.*,

Record-high mobility and extreme magnetoresistance on kagome-lattice in compensated semimetal Ni3In2S2, Science China Materials **66** (2023).